Nano electro-mechanical optoelectronic tunable VCSEL

Michael C.Y. Huang, Ye Zhou, and Connie J. Chang-Hasnain

Department of Electrical Engineering and Computer Science, University of California, Berkeley, California 94720
cch@eecs.berkeley.edu

Abstract: We report a novel electrostatic actuated nano-electromechanical optoelectronic (NEMO) tunable vertical-cavity surface-emitting laser (VCSEL) centered at 850 nm. By integrating a movable, single-layer (230 nm), high-index-contrast subwavelength grating (HCG) as the VCSEL top mirror, single mode emission (SMSR >40 dB) and continuous wavelength tuning (~2.5 nm) was obtained at room temperature under CW operation. The small footprint of HCG enables the scaling down of each of the cantilever dimensions by a factor of 10, leading to 1000 times reduction in mass, which potentially increases the mechanical resonant frequency and tuning speed.

OCIS codes: (250.7260) Vertical-cavity surface-emitting lasers; (140.3600) Tunable Laser

References and Links

1. C. J. Chang-Hasnain, "Tunable VCSEL," IEEE J. Select. Top. Quantum Electron. **6**, 978-987 (2000).
2. J. S. Harris, Jr., "Tunable long-wavelength vertical-cavity lasers: the engine of next generation optical networks?" IEEE J. Select. Top. Quantum Electron. **6**, 1145-1160 (2000).
3. C. F. R. Mateus, M. C. Y. Huang, C. J. Chang-Hasnain, J. E. Foley, R. Beatty, P. Li, and B. T. Cunningham, "Ultra-sensitive immunoassay using VCSEL detection system," Electron. Lett. **40**, 649-651 (2004).
4. M. Lackner, M. Schwarzott, F. Winter, B. Kogel, S. Jatta, H. Halbritter, and P. Meissner, "CO and CO_2 spectroscopy using a 60 nm broadband tunable MEMS-VCSEL at 1.55um," Opt. Lett. **31**, 3170-3172 (2006).
5. J. Kitching, "Miniature atomic clock makes its debut," Opto & Laser Europe, 22-23 (2004).
6. S. Decai, W. Fan, P. Kner, J. Boucart, T. Kageyama, Z. Dongxu, R. Pathak, R. F. Nabiev, and W. Yuen, "Long wavelength-tunable VCSELs with optimized MEMS bridge tuning structure," IEEE Photon. Technol. Lett. **16**, 714-716 (2004).
7. F. Riemenschneider, M. Maute, H. Halbritter, G. Boehm, M. C. Amann, and P. Meissner, "Continuously tunable long-wavelength MEMS-VCSEL with over 40-nm tuning range," IEEE Photon. Technol. Lett. **16**, 2212-2214 (2004).
8. M. C. Y. Huang, K. B. Cheng, Z. Ye, B. Pesala, C. J. Chang-Hasnain, and A. P. Pisano, "Demonstration of piezoelectric actuated GaAs-based MEMS tunable VCSEL," IEEE Photon. Technol. Lett. **18**, 1197-1199 (2006).
9. C. F. R. Mateus, M. C. Y. Huang, and C. J. Chang-Hasnain, "Micromechanical tunable optical filters: general design rules for wavelengths from near-IR up to 10um," Sens. Actuators A **119**, 57-62 (2005).
10. C. F. R. Mateus, M. C. Y. Huang, D. Yunfei, A. R. Neureuther, and C. J. Chang-Hasnain, "Ultrabroadband mirror using low-index cladded subwavelength grating," IEEE Photon. Tech. Lett. **16**, 518-520 (2004).
11. C. F. R. Mateus, M. C. Y. Huang, C. Lu, C. J. Chang-Hasnain, and Y. Suzuki, "Broad-band mirror (1.12-1.62 um) using a subwavelength grating," IEEE Photon. Technol. Lett. **16**, 1676-1678 (2004).
12. C. Lu, M. C. Y. Huang, C. F. R. Mateus, C. J. Chang-Hasnain, and Y. Suzuki, "Fabrication and design of an integrable subwavelength ultrabroadband dielectric mirror," Appl. Phys. Lett. **88**, 31102 (2006).
13. M. C. Y. Huang, Y. Zhou, and C. J. Chang-Hasnain, "A surface emitting laser incorporating a high-index-contrast subwavelength grating," Nature Photon. **1**, 119-122 (2007).
14. H. G. Craighead, "Nanoelectromechanical systems," Science **290**, 1532-1535(2000).
15. M. G. Moharam and T. K. Gaylord, "Rigorous coupled-wave analysis of planar-grating diffraction," J. Opt. Soc. Am. **71**, 811-818 (1981).

#76416 - $15.00 USD Received 31 October 2006; revised 17 January 2007; accepted 17 January 2007

1. Introduction

The integration of micro-electromechanical structures (MEMS) with vertical-cavity surface-emitting lasers (VCSELs) have been extensively studied as an ideal wavelength tunable source for a variety of applications, including telecommunication [1, 2], biomolecular or chemical sensing [3] , spectroscopy [4], and chip-scale atomic clock [5]. MEMS tunable structures are desirable because they provide a large and continuous tuning range with precise mechanical displacement control. Recently, there has been exciting research work in the area of MEMS tunable VCSELs, with a special emphasis in increasing their wavelength tuning range [6-8]. However for conventional VCSELs, the distributed Bragg reflector (DBR) thickness of 3-10 μm (or equivalently 4-6 λ) imposes a significant design trade-off on the tuning speed, wavelength range, actuation voltage, as well as fabrication difficulties [9]. Recently, we proposed a new class of high-reflectivity mirror using a single-layer (thickness 0.23 μm or equivalently 0.27 λ for center wavelength of 850 nm) high-index-contrast subwavelength grating (HCG) instead of conventional DBR [10-12]. The design consists of only ONE single layer of grating structure of high refractive index material entirely surrounded by low index material (e.g. air). Using this design, a VCSEL can be fabricated using a HCG-based top mirror with thickness <10% of that for conventional DBR [13].

Here, we present a novel electrostatic nano-electromechanical structured (NEMO) tunable surface emitting laser using a movable electrostatic-actuated HCG, for the first time. The NEMO structure is scaled down by a factor of 10 times in all dimensions, and hence the mass is <0.1% of regular DBR-based MEMS. For a similar thickness-length ratio, this yields a similar spring constant with a much smaller mass, resulting in a smaller tuning voltage and a much faster tuning speed [14]. As mechanical resonant frequency is inversely proportional to the square root of mass, the 1000 times reduction in mass can lead to more than 30 times improvement in the tuning speed. In addition, the design can be readily adapted for a variety of optoelectronic wavelength-tunable MEMS devices operating at a variety of different wavelength regimes.

2. Design

Figure 1 shows the cross-section schematic of the electrostatic actuated NEMO tunable VCSEL. The device consists of 34 pairs of bottom *n*-doped DBRs, a λ-cavity layer with GaAs quantum well active region, and a HCG-based top mirror. The top mirror is comprised of three parts (starting from the substrate side): a fixed 4 pairs of *p*-doped DBR, a variable airgap, and a freely suspended *n*-doped HCG that is supported via a nano-mechanical cantilever. The 4 pairs of fixed *p*-DBRs are used for the purpose of electrical current injection and protection from fabrication processes. While the p-DBR does increase the overall reflectivity of the top mirror, our simulation shows that the number of p-DBR pairs can be reduced since a single-layer HCG is capable for providing sufficient reflectivity (R>99.9%) as the VCSEL top mirror.

The structure of the HCG consists of periodic stripes of $Al_{0.6}Ga_{0.4}As$ that are freely suspended with air as the low-index cladding layers on the top and bottom. The grating is composed of the following parameters: period (Λ) = 0.375 μm, grating thickness (t_g) = 0.235 μm, duty cycle (DC) = 65%, airgap thickness (t_L) = 1.05 μm ($5\lambda/4$), and area = 10 μm x10 μm. Duty cycle is defined as the ratio of the width of the high index material to Λ. The airgap is formed by selectively removing the sacrificial layer material (undoped GaAs) underneath the grating and cantilever.

#76416 - $15.00 USD Received 31 October 2006; revised 17 January 2007; accepted 17 January 2007

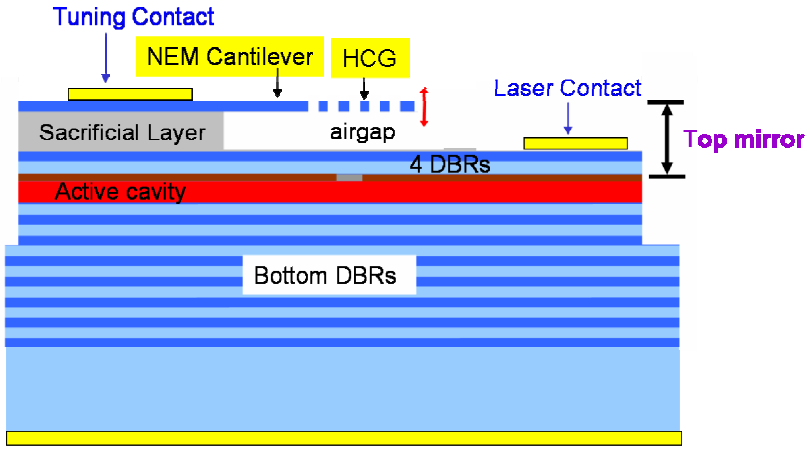

Fig.1. Schematic cross-section of NEMO tunable VCSEL. The top mirror consists of a fixed 4 pairs of p-doped DBR, a variable airgap, and a freely-suspending n-doped high-index-contrast subwavelength grating (HCG) that is supported via a nano-cantilever beam.

For this optical cavity design, we simulated the reflectivity of the composite top mirror using rigorous coupled wave analysis method [15], as shown in Fig. 2. For the normal-incident TM polarized light with the electric field perpendicular to grating stripes, the reflectivity is >99.9% for wavelength ranges of 0.8-0.88 μm, meanwhile the reflectivity is only about 95% for the TE polarized light with the electric field parallel to the grating stripes. The reflectivity difference for the two polarizations resides on the differences in boundary conditions and consequently can be use to select a pre-defined emission polarization of the VCSEL [13]. Since a reflectivity value of 99.5% is typically required for a VCSEL to achieve lasing, consequently the HCG is an excellent candidate for serving as the top mirror of a VCSEL with the added benefit of polarization control that is not attainable for conventional DBRs. In comparison, the reflectivity for the VCSEL top mirror with an HCG of grating duty cycle of 0% (R = 70%) and 100% (R = 90%) are also shown. A duty cycle of 0% corresponds to no HCG layer (only 4 pairs of fixed DBRs), while a duty cycle of 100% means an additional uniform layer of AlGaAs is used to provide extra reflectivity.

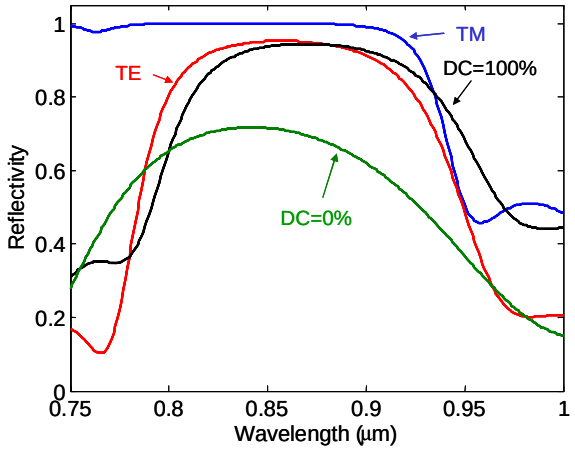

Fig. 2. Simulated reflectivity for the NEMO HCG-based top mirror (duty cycle of 65%). The reflectivity is >99.9% for normal-incident TM polarized light for wavelength ranges of 0.8-0.88 μm, meanwhile the reflectivity is merely 95% for TE polarized light. In comparison, the reflectivity for a HCG with a grating duty cycle of 0% and 100% is also shown.

#76416 - $15.00 USD Received 31 October 2006; revised 17 January 2007; accepted 17 January 2007

Electric current injection is conducted through the middle contact (via the *p*-doped DBR) and backside contact. An aluminum oxide aperture is formed on an AlAs layer in the *p*-DBR section immediately above the cavity layer to provide efficient current and optical confinement. The tuning contact is fabricated on the top *n*-doped HCG layer. Wavelength tuning is accomplished by applying a reverse voltage bias across the top *n*-doped HCG layer and the middle *p*-DBR. The reverse voltage results in an electric field across the airgap, which attracts the cantilever toward substrate. This produces a mechanical deflection that reduces the airgap size, which then varies the Fabry-Perot resonance of the cavity and hence blue-shifts the emission wavelength of the VCSEL.

The fabrication process includes three sequential metal depositions, two vertical etches for structure formation, thermal oxidation, and one vertical followed by selective etch for HCG formation. The HCG was patterned by electron-beam lithography on poly-methyl methacrylate (PMMA) photoresist, which enables proper alignment to the oxide aperture and the design flexibility in terms of varying the grating period and duty cycle. However, given the current state-of-art lithography technology, the HCG can also be readily defined by more efficient and low-cost methods such as nano-imprinting. A wet chemical-based selective etching followed by critical point drying was required to remove the sacrificial material underneath the HCG layer and form the freely suspending grating structure that is supported by a nano-cantilever beam. Comparing to the conventional RIE-based selective etch method, the chemical based selective etching enables very rapid fabrication cycle with very high etch selectivity and improves the device yield and reproducibility. Figure 3(a) and 3(b) shows the SEM image of the fabricated device, where all of the geometric dimensions (length, width and thickness) are <10% of conventional MEMS devices. Consequently, the mass of the cantilever is >1000x smaller. The inset in Fig. 3(b) shows the zoomed-in image of the fabricated grating fingers, which is freely suspended and supported by two cantilevers.

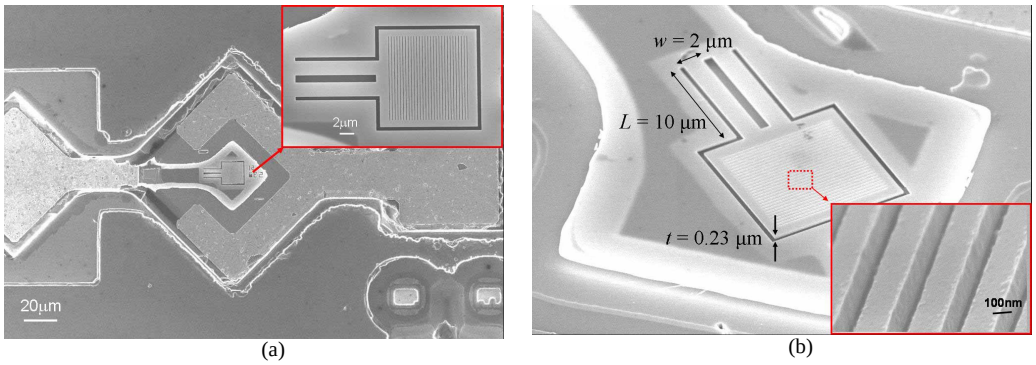

(a) (b)

Fig. 3. Scanning electron microscope image of fabricated device. (a) Top view showing the entire device structure and the inset shows the zoo-in image of the HCG in the middle of the VCSEL mesa. (b) Side-view focusing on the freely-suspended HCG that is supported via a nano-cantilever, and the inset shows the zoom-in image of individual grating fingers.

3. Results

With the HCG integrated as the top mirror, continuous wave (CW) operation of an electrostatic actuated NEMO tunable VCSEL was demonstrated for the first time at room temperature. Figure 4(a) shows the VCSEL static characteristics (without applying the tuning voltage), for output power versus bias current (LI) and voltage versus bias current (IV) relations. The device exhibits a lasing threshold current of 1.3 mA and an output power ~0.5 mW when biased at 2.3 times I_{th} with the slope efficiency of 0.3 mW/mA. Figure 4(b) shows the measured emission spectrum of the device centered at 861 nm under a bias current of 1.3 times I_{th}. Single mode emission with a side-mode suppression ratio (SMSR) of over 40 dB was obtained, which can be accounted by both the aluminum oxide optical confinement and area-dependent reflectivity of the HCG that suppresses higher-order transverse modes.

#76416 - $15.00 USD Received 31 October 2006; revised 17 January 2007; accepted 17 January 2007

Currently the device performance is mainly limited by contact and series resistance. Lower threshold (<1 mA) and larger output power (>1 mW) device can be attained with future optimization of the fabrication process.

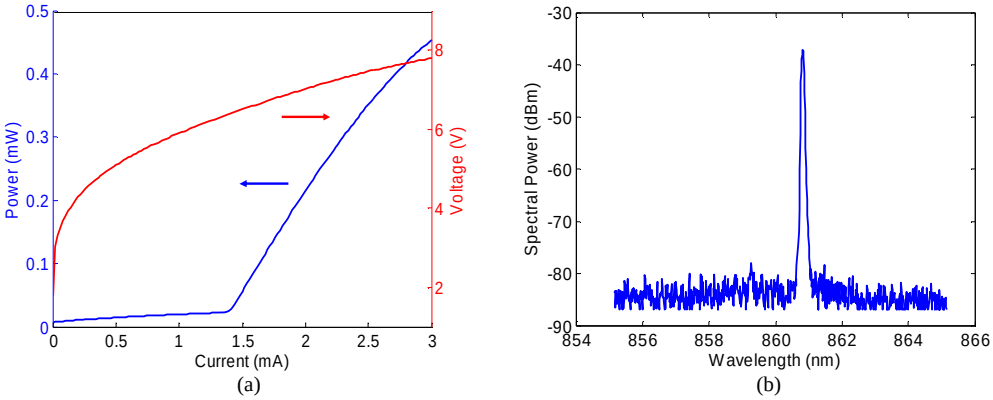

Fig. 4. Measured continuous-wave (CW) static characteristics of the NEMO tunable VCSEL without applying external bias voltage. (a) Light-intensity versus bias (LI) and electrical voltage versus current (IV) characteristic of the fabricated device. (b) Emission spectrum of the device biased at 1.3 times the threshold current.

When applying a reverse bias voltage across the tuning contacts, the electrostatic force deflects the cantilever beam, which translates to a decrease in the laser emission wavelength. Due to light mass of the structure, ultra-low actuation power (<50 nW) is required to actuate the cantilever, which is 1000 times smaller than that for the conventional MEMS tunable VCSEL. Figure 5(a) shows the CW emission tuning spectra of the device when the active region is electrically pumped at 1.8 times I_{th}, with various applied voltage across the tuning contact. A continuous wavelength tuning range of ~2.5 nm was obtained towards shorter wavelength. The laser emission remains single mode output throughout the entire tuning range. Figure 5(b) shows the emission wavelength as a function of the applied voltage and the corresponding spectral intensity under those tuning conditions. The wavelength tuning exhibits a quadratic-like behavior known to typical electrostatic actuation. In addition, the emission spectral intensity remains fairly constant throughout most of the tuning range.

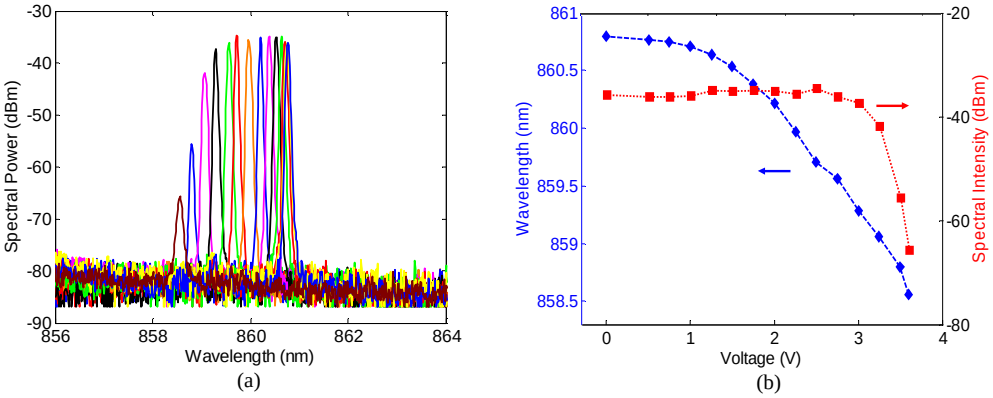

Fig. 5. (a) CW tuning spectra for the NEMO tunable VCSEL under various external applied voltages across the HCG cantilever. (b) Measured emission wavelength as a function of applied external voltage and measured peak spectral intensity as a function of applied voltage.

#76416 - $15.00 USD Received 31 October 2006; revised 17 January 2007; accepted 17 January 2007

To characterize the mechanical deflection, we measured the physical displacement of the nano-cantilever beam as a function of applied voltage using a white light interferometer, as shown in Fig. 6(a). The deflection follows a quadratic behavior similar to Fig. 5(b), and a maximum mechanical deflection of 350 nm was obtained by applying external bias voltage up to 4.5V, before pull-in occurred. Furthermore, to estimate the wavelength tuning of the NEMO tunable VCSEL, we simulated the Fabry-Perot resonant wavelength of the device in respect to the variations in the airgap, as shown in Fig. 6(b). For an applied voltage of 3.5V (from Fig. 5(b)), the thickness of airgap changes from 1.1 to 0.9 μm. Within this range of airgap, the simulation result shows that the expected wavelength shift is about 4 nm, which is fairly close in agreement with our experimentally obtained ~2.5 nm wavelength shift. Further improvement of the wavelength tuning can be achieved by increasing the allowable physical mechanical deflection with a larger initial air gap size (and hence a larger Δd_{airgap}); and improving the wavelength tuning efficiency ($\Delta\lambda/\Delta d_{airgap}$) by operating on the steeper part of $\Delta\lambda/\Delta d_{airgap}$ curve and/or with a reduced the number of p-DBRs to get a larger $\Delta\lambda/\Delta d_{airgap}$ value.

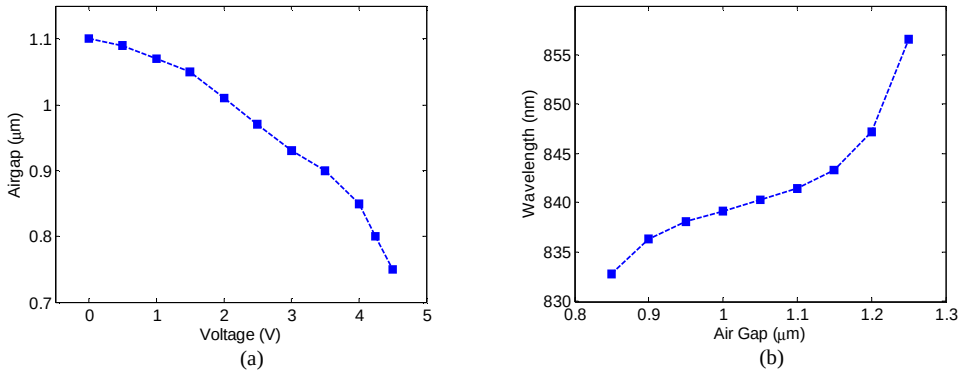

Fig. 6. (a) Measured mechanical deflection of the cantilever beam under various external applied voltages using a white light interferometer. (b) Simulated VCSEL emission wavelength as a function of airgap thickness.

4. Conclusion

The nano-electromechanical optoelectronic tunable VCSEL described here is achieved by integrating a movable, freely-suspending, single-layer, high-index-contrast subwavelength grating with a vertical-cavity surface-emitting laser. The small footprint of HCG enables the scaling down of the cantilever geometric dimensions, which results in 1000 times reduction in mass and hence the increase in its mechanical resonant frequency. By using electrostatic actuation to control the airgap spacing, precise and continuous wavelength tuning of ~2.5 nm was obtained with an ultra-low actuation power (<50 nW). The simplicity, wavelength-scalability, and versatility of the single-layer HCG design would provide numerous benefits for making wavelength-tunable optoelectronic devices such as VCSELs, optical filters and detectors for a wide range of wavelengths.

Acknowledgments

This work has been supported by the DARPA Center for Optoelectronic Nanostructured Semiconductor Research and Technology (CONSRT) HR0011-04-1-0040.

#76416 - $15.00 USD Received 31 October 2006; revised 17 January 2007; accepted 17 January 2007